ChemPhysChem

Chemistry Europe
European Chemical Societies Publishing

Accepted Article

Title: Tuning Molecular Electron Affinities against Atomic Electronegativities by Spatial Expansion of a π-System

Authors: Elena A. Chulanova, Ekaterina A. Radiush, Nikolay A. Semenov, Emanuel Hupf, Irina G. Irtegova, Yulia S. Kosenkova, Irina Yu. Bagryanskaya, Leonid A Shundrin, Jens Beckmann, and Andrey V. Zibarev

To be cited as: *ChemPhysChem* **2023**, e202200876

Link to VoR: https://doi.org/10.1002/cphc.202200876

WILEY-VCH

RESEARCH ARTICLE WILEY-VCH

Tuning Molecular Electron Affinities against Atomic Electronegativities by Spatial Expansion of a π-System

Elena A. Chulanova,[a,c] Ekaterina A. Radiush,[a] Nikolay A. Semenov,[a] Emanuel Hupf,[b] Irina G. Irtegova,[a] Yulia S. Kosenkova,[a] Irina Yu. Bagryanskaya,[a] Leonid A. Shundrin,*[a] Jens Beckmann,*[b] and Andrey V. Zibarev*[a]

[a] Dr. E. A. Chulanova, E. A. Radiush, Dr. N. A. Semenov, Dr. I. G. Irtegova, Dr. Yu. S. Kosenkova, Prof. Dr. I. Yu. Bagryanskaya, Prof. Dr. L. A. Shundrin, Prof. Dr. A. V. Zibarev
Novosibirsk Institute of Organic Chemistry
Siberian Branch of the Russian Academy of Sciences
630090 Novosibirsk (Russian Federation)
E-mail: zibarev@nioch.nsc.ru (A. V. Z.); shundrin@nioch.nsc.ru (L. A. S.)

[b] Dr. E. Hupf, Prof. Dr. J. Beckmann
Institute for Inorganic Chemistry and Crystallography
University of Bremen
28359 Bremen (Germany)
E-mail: j.beckmann@uni-bremen.de (J. B.)

[c] Dr. E. A. Chulanova
Institute for Applied Physics
University of Tübingen
72076 Tübingen (Germany

Supporting information for this article is given via a link at the end of the document.

Abstract: With 2,1,3-benzochalcogenadiazoles $C_6R_4N_2E$ (**E/R**; E = S, Se, Te; R = H, F, Cl, Br, I) and $C_6H_2R_2N_2E$ (**E/R'**; E = S, Se, Te; R = Br, I) – 10π-electron hetarenes, it is shown by CV / EPR measurements, DFT calculations, and QTAIM and ELI-D analyses that their molecular electron affinities (EAs) increase with decreasing Allen electronegativities and electron affinities of the E and non-hydrogen R (except Cl) atoms. DFT calculations for **E/R** + $e^- \rightarrow [E/R]^-$ electron capture reveal negative ΔG values numerically increasing with increasing atomic numbers of the E and R atoms; positive ΔS has a minor influence. It is suggested that the increased EAs are caused by more effective charge / spin delocalization in the radical anions of heavier derivatives due to contributions from diffuse (a real-space expanded) p-AOs of the heavier E and R atoms; and that this counterintuitive effect might be of the general character.

Introduction

A charge transfer (CT) between electron-donor and electron-acceptor species is important for chemistry and materials science. Incomplete CT leads to polarized molecular complexes, and complete CT to radical-ion salts. Frequently, the former reveal properties of molecular conductors; and the latter, molecular magnets.[1-3] Generally, CT is considered to be one of the prevailing switching mechanisms of memristors (memory resistors) based on organic polymers[4,5] and also plays a crucial role in the processes of exciton dissociation, charge separation and charge recombination in solar cells.[6]

One of the most widely used descriptors of the electron-acceptor ability (EAA) is the electronegativity χ.[7-9] There are numerous definitions of χ, some of which have a clear physical meaning, particularly those by Mulliken and Allen – χ_M[10] and χ_A,[11] respectively. Consequently, χ_M and χ_A can be measured experimentally as real physical properties of species. Generally, higher χ's values lead to a higher EAA of the species.

Here we report on an unexpected reversed trend observed with 2,1,3-benzochalcogenadiazoles **E/H** and their 4,5,6,7-tetrahalogen and 4,7-dihalogen derivatives **E/R** and **E/R'**, respectively (Scheme 1). We have found that the EAA of these compounds, assessed experimentally with CV / EPR and theoretically with DFT, QTAIM and ELI-D, increases with decreasing χ_A and electron affinities of the E and non-hydrogen R (except Cl) atoms; and for the halogenated derivatives, with a decrease of χ_M of molecules. As a result, the strongest electron acceptor amongst the theoretically characterized compounds and overall in the series is **Te/I**; and amongst experimentally characterized compounds, **Te/Cl** (Scheme 1).

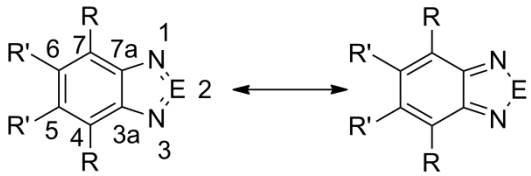

E/H: E = S, Se, Te; R, R' = H
E/F: E = S, Se, Te; R, R' = F
E/Cl: E = S, Se, Te; R, R' = Cl
E/Br: E = S, Se, Te; R, R' = Br
E/I: E = S, Se, Te; R, R' = I
E/Br': E = S, Se, Te; R = Br, R' = H
E/I': E = S, Se, Te; R = I, R' = H

Scheme 1. 2,1,3-Benzochalcogenadiazoles represented by superposition of the benzoid and quinoid forms, together with atom numbering; relative contribution of the forms depends on E.[12]

It should be noted that compounds **E/H**, **E/R** and **E/R'**, which are 10π-electron hetarenes, are widely used in contemporary chemistry and materials science due to a unique set of properties including high EAA, dualistic Lewis ambiphilicity; enhanced chromophoric / fluorophoric performances; redox activity; and a propensity to secondary bonding interactions with special emphasis on chalcogen bonding.[12-20] In some fundamental and applied aspects their EAA, highlighted by the formation of CT complexes and radical anions (RAs), plays the key role.[13,18-26]

The new effect described in this work clarifies some earlier unexplained findings, e. g. regarded to the EAA of C_6R_6 benzene derivatives (R are the same as above). More important, it might be of the general character for π-cyclic heteroatom compounds and find applications in the design and synthesis of new molecular conductors (CT complexes) and magnets (RA salts).

Results and Discussion

Two sets of compounds are studied (Scheme 1): 1) the archetypal 2,1,3-benzochalcogenadiazoles and their 4,5,6,7-tetrahalogen derivatives **E/R**, and 2) 4,7-dihalogen derivatives **E/R'** (Table 1, Figure 1; ESI). Compounds **Te/Br** and **Te/I** are not involved into experimental study due to the lack of suitable synthetic methods and the presumably low solubility in organic solvents caused by strong Te…N chalcogen bonding,[27,28] which prevents CV measurements. The influence of the iodine is studied experimentally with compounds **E/I'** in comparison with compounds **E/Br'**. With CV, the first reduction half-wave potentials $E_{1/2}$[29] are measured in DMF and MeCN solvents; and onset potentials E_{on}[30-32] in DMF under the same conditions (ESI). The electrochemically obtained $[\mathbf{E/R}]^{\cdot-}$ and $[\mathbf{E/R'}]^{\cdot-}$ persistent RAs are characterized by EPR and DFT (ESI).

Table 1. Compounds **E/R**: the experimental first reduction half-wave potentials $E_{1/2}$ and onset potentials E_{on} in solution;[a-c] gas-phase DFT adiabatic and vertical electron affinities aEA$_1$ and vEA$_1$, and vertical ionization energies vIE$_1$;[d-f] Mulliken and Allen electronegativities χ_M and χ_A;[g,h] and atomic electron affinities.[i]

Compounds	$E_{1/2}$ / MeCN	E_{on} / DMF	$E_{1/2}$ / DMF	aEA$_1$	vEA$_1$	vIE$_1$ (exp.[33,34])	χ_M
S/H	–1.53[20]	–1.33	–1.42	0.82	0.68	8.85 (8.98)	4.77
Se/H	–1.37[20]	–1.19	–1.28	1.02	0.89	8.65 (8.80)	4.77
Te/H	–1.24[20]	–1.06	–1.18	1.12	1.00	8.57 (8.57)	4.79
S/F	–1.21	–0.94	–1.03	1.45	1.24	9.18 (9.51)	5.21
Se/F	–1.08	–0.81	–0.93	1.63	1.44	8.97 (9.28)	5.21
Te/F	–	–0.72	–0.79[j]	1.70	1.52	8.70	5.11
S/Cl[k]	–1.01	–0.78	–0.87	1.69	1.54	8.64	5.09
Se/Cl[k]	–0.89	–0.71	–0.78	1.85	1.71	8.48	5.10
Te/Cl	–	–0.63	–0.71[j]	1.90	1.78	8.27	5.03
S/Br	–	–0.79	–0.87	1.79	1.65	8.48	5.06
Se/Br	–	–0.71	–0.79	1.95	1.82	8.34	5.08
Te/Br	–	–	–	2.00	1.88	8.15	5.02
S/I	–	–	–	1.85	1.68	8.05	4.87
Se/I	–	–	–	1.98	1.86	7.94	4.90
Te/I	–	–	–	2.04	1.93	7.77	4.85

[a] From CV in MeCN and DMF with respect to saturated calomel electrode (SCE), V. [b] Taking into account the approximate proportionality of the change in re-solvation energies $\delta\Delta G_{solv}$ in each **E/Hal** subset, the main contribution *to the change* in the corresponding $E_{1/2}$ / E_{on} can be associated with gas-phase EAs of molecules.[35] [c] From CV in DMF with Pt working electrode at the potential sweep rate of 0.1 V·s^{-1} with respect to SCE, V (ESI). [d] Fully-optimized gas-phase (U)B3LYP/def2-tzvp calculations with ECP for Te and I, eV. [e] $EA_1 = E(M) – E(M^{\cdot-})$. When positive, EA_1 represents stabilization of $[M]^{\cdot-}$ with respect to M in the $M + e^{\cdot-} \rightarrow [M]^{\cdot-}$ gas-phase process, in which vertical transition occurs to $[M]^{\cdot-}$ in non-relaxed geometry and adiabatic transition to $[M]^{\cdot-}$ in energetically more favorable relaxed geometry, and aEA$_1$ > vEA$_1$. [f] $IE_1 = E(M^{\cdot+}) – E(M)$. [g] $\chi_M = ½(v\text{EA}_1 + v\text{IE}_1)$, eV. [h] On Pauling scale, χ_A = 2.59, 2.42 and 2.16 for S, Se and Te, respectively; and 4.19, 2.87, 2.69 and 2.36 for F, Cl, Br and I, respectively. For H, χ_A = 2.30. [i] Atomic electron affinity, eV, is 2.08, 2.02 and 1.97 for S, Se and Te, respectively; and 3.40, 3.62, 3.36 and 3.06 for F, Cl, Br and I, respectively; for H, 0.75.[36] [j] Calculated using CV simulations (ESI). [k] For the CVs in MeCN (ESI).

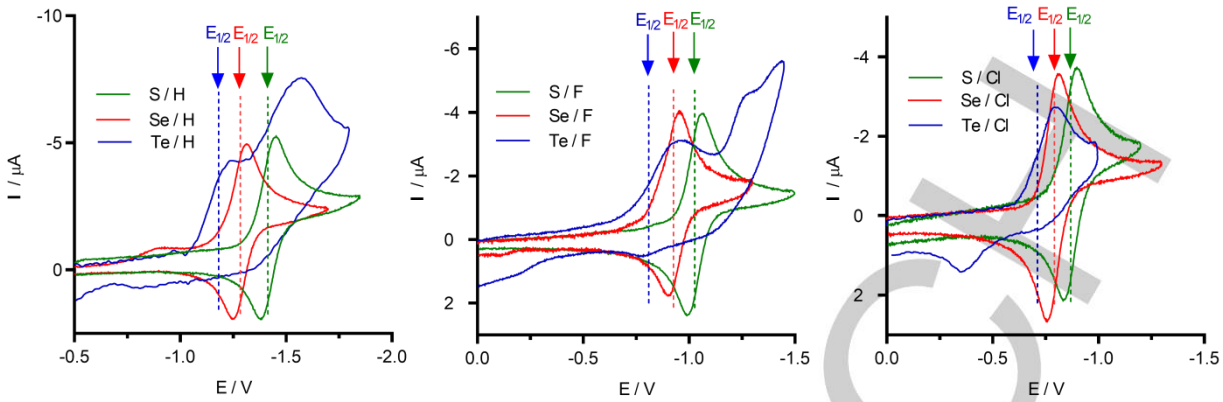

Figure 1. CVs of compounds **E/R** in DMF at ν = 0.1 V·s^{-1} normalized to equal concentration of 1 mM (for determining $E_{1/2}$ of **Te/R**, see ESI).

Table 2. Compounds **E/R'**: the experimental first reduction half-wave potentials $E_{1/2}$ in solution;[a] gas-phase DFT adiabatic and vertical electron affinities aEA$_1$ and vEA$_1$,[b,c] and vertical ionization energies vIE$_1$;[d] and Mulliken electronegativities χ_M.[e]

Compounds	$E_{1/2}$	aEA$_1$	vEA$_1$	vIE$_1$	χ_M
S/Br'	–1.05	1.46	1.30	8.48	4.89
Se/Br'	–0.95	1.63	1.49	8.34	4.92
Te/Br'	–0.93	1.70	1.57	8.14	4.86
S/I'	–1.06	1.50	1.35	8.17	4.76
Se/I'	–0.98	1.68	1.54	8.05	4.80
Te/I'	–0.98	1.75	1.62	7.89	4.75

[a] From CV in DMF with respect to SCE, V. [b] Fully-optimized gas-phase (U)B3LYP/def2-tzvp calculations with ECP for Te and I, eV. [c] EA$_1$ = E(M) – E(M$^-$). [d] vIE$_1$ = E(M$^+$) – E(M). [e] χ_M = ½(vEA$_1$ + vIE$_1$), eV.

It is found that the EAA of **E/R** and **E/R'** represented by $E_{1/2}$ and E_{on} potentials increases with a decrease of χ_A of both E and R atoms (and their atomic EA, except for Cl); and for **E/Hal**, that the trend is also tracked with χ_M of the molecules. Overall, the strongest electron acceptor amongst experimentally studied compounds is **Te/Cl** with $E_{1/2}$ / E_{on} = –0.71 / –0.63 V (DMF); and amongst computationally studied compounds and in the whole series, **Te/I** with aEA$_1$ = 2.04 eV (Tables 1 and 2; ESI).

The gas-phase DFT-calculated change of the Gibbs free energy ΔG for the **E/R** + e$^-$ → [**E/R**]$^-$ electron capture is negative and numerically increasing with the atomic numbers of both E and R atoms (ESI). The determining factor for aEA$_1$ is ΔH, which is typical of organic gas-phase electron-transfer reactions.[36,37] Positive and E-dependent ΔS has a minor influence on aEA$_1$ for **E/R** with R = H, F, Cl, Br, becoming, however, more significant with R = I. The latter leads to a deviation from the linear correlation between $-\Delta G$ and aEA$_1$, which is as follows: $-\Delta G$ = (0.9557 ± 0.018)·aEA$_1$ – 0.057 for the full set of compounds; and $-\Delta G$ = (1.033 ± 0.058)·aEA$_1$ + 0.034 when **E/I** are omitted (for graphical representation, see ESI).

On transformation of **E/R** into [**E/R**]$^{\cdot-}$, the π*-LUMOs of the former, which are isolobal for the whole series, transforms into the π*-SOMOs of the latter (ESI). The spatial expansion of these MOs is controlled by the contribution from p-AOs of E and R atoms in accordance with their covalent[38] and van der Waals (VdW)[39-41] radii (with Penning ionization electron spectroscopy of C_6H_5R benzene derivatives (R = F, Cl, Br, I), it is seen that π-MOs expand even outside the molecular VdW surfaces).[42] This real-space gradual expansion increases delocalization of the unpaired electron and progressively stabilize corresponding [**E/R**]$^-$ containing heavier E and R atoms, *i.e.*, increases EA$_1$ of their neutral precursors **E/R**. Overall, it is suggested that the discovered effect is caused by a more effective charge / spin delocalization in the π*-SOMOs of RAs of the compounds due to contributions from diffuse p-AOs of the heavier E and R atoms; and thermodynamic stabilization on going from **E/R** to [**E/R**]$^-$ can be associated with lower electrostatic repulsion in [**E/R**]$^-$. Conceptually, this effect belongs to size-dependent effects in chemistry.

The gradual increase of the EAA with the gradual spatial expansion of a molecular π-system is known, e. g. for acenes,[43] where it requires spatial expansion of a molecular scaffold via increasing the number of C atoms with the same χ (*i.e.*, naphthalene → anthracene → tetracene → pentacene, etc.). This is not the case for **E/R** and **E/R'** whose scaffold remains unchanged but χ_A is varied.

The formation of [**E/R**]$^-$ is ultimate manifestation of the EAA of **E/R**, and [**E/R**]$^-$ worth in-depth consideration. DFT-calculated Mulliken[44] and QTAIM[45,46] distributions of atomic charges and spin densities in [**E/R**]$^-$ confirm that a whole molecule participates in charge / spin delocalization despite Mulliken and QTAIM patterns are quite different (ESI).[47] The QTAIM and ELI-D[48,49] analyses disclose important stereoelectronic changes on going from **E/R** to [**E/R**]$^-$ (Figure 2; ESI). Particularly, upon the **E/R** + e$^-$ → [**E/R**]$^-$ electron capture, the electron density of the E–N bonds decrease and the Laplacian become more negative indicating pronounced covalent character in [**E/R**]$^-$ *vide supra*. In conjunction, the $G/\rho(r)_{cp}$ values are significantly more positive in **E/R**. However, the $H/\rho(r)_{cp}$ values are actually also more negative in **E/R** compared to [**E/R**]$^-$ indicating the presence of both, pronounced ionic and covalent, E–N bonding aspects in **E/R**. This effect is more significant in the S compounds compared to the heavier

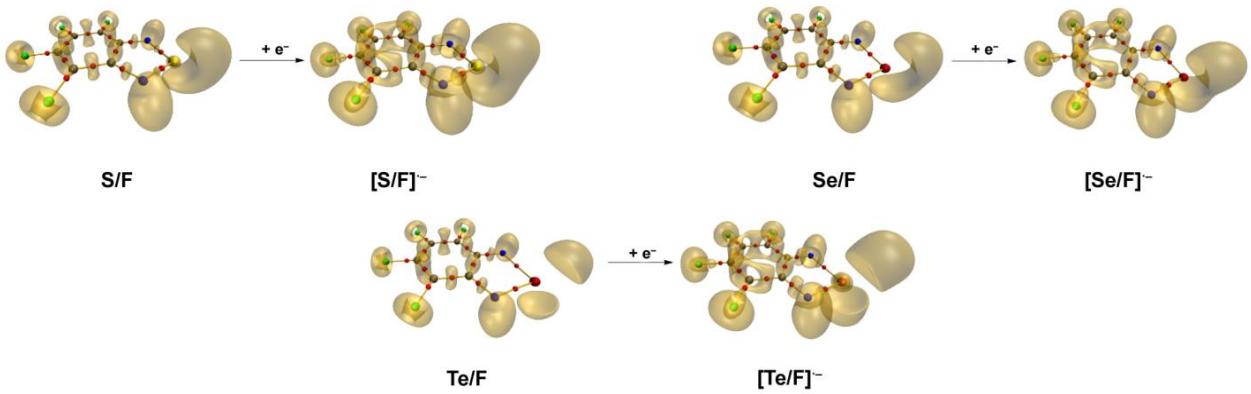

Figure 2. QTAIM bond paths of **E/F** and [**E/F**]$^{\cdot-}$ with *cp*'s given as red dots, and ELI-D localization domains depicted in transparent mode at *iso*-values of 1.50.

Se/Te species. With the QTAIM bond[45,46] / line[50] critical points (below denoted as *cp*'s), the covalent character of the E–N bond decreases in the order S–N > Se–N > Te–N in both **E/R** and [**E/R**]$^{\cdot-}$ species. Particularly, this is exemplified by negative Laplacians for **S/R** ($\nabla^2\rho(\mathbf{r})_{cp}$ = –7.0 to –7.8 e Å^{-5}) and [**S/R**]$^{\cdot-}$ ($\nabla^2\rho(\mathbf{r})_{cp}$ = –8.6 to –10.1 e Å^{-5}), respectively. These are more negative compared to Se and Te congeners showing Laplacians of $\nabla^2\rho(\mathbf{r})_{cp}$ = –0.3 to 0.0 e Å^{-5} (**Se/R**) and –0.6 to –1.0 e Å^{-5} ([**Se/R**]$^{\cdot-}$); as well as, $\nabla^2\rho(\mathbf{r})_{cp}$ = +4.6 to +4.2 e Å^{-5} (**Te/R**), and +3.8 to +3.0 e Å^{-5} ([**Te/R**]$^{\cdot-}$). Covalent interactions are also indicated by negative values of the total energy density over $\rho(r)_{cp}$ ratios ($H/\rho(r)_{cp}$) and consequently those ratios show the most negative values for the S derivatives, followed by the Se derivatives and are less negative for the Te derivatives. It should also be stated that the electron density at the E–N *cp*'s decreases in the order S > Se > Te. Simultaneously, pronounced ionic contributions are reflected by strongly positive kinetic energy density over $\rho(r)_{cp}$ ratios ($G/\rho(r)_{cp}$) and in conjunction those values increase in the order S–N > Se–N > Te–N (ESI).

The ELI-D electron population analysis reveals increasing lone pair populations for N and E atoms in [**E/R**]$^{\cdot-}$ as compared with **E/R**. In agreement with the spin density consideration, all atoms are participating in the electron-capture process and the population of the V_2(C5–C6), V_2(C3*a*–C4) and V_2(C7*a*–C7) bonding basins are increasing, whereas the population of the V_2(C–N), V_2(C4–C5) and V_2(C6–C7) bonding basins are decreasing and the bridging V_2(C3*a*-C7*a*) show similar populations in the **E/R** and [**E/R**]$^{\cdot-}$ species. This effect is more pronounced for R = H and F and decreases steadily for heavier R (ESI).

Molecular electrostatic potential (MEP)[51] of the **E/R** compounds reveals expected σ-holes[52] at the heavier E and R atoms, together with π-holes[52] at the hetero- and carbo-cycles of the heavier derivatives. However, energy of electrostatic interaction of a free electron with π-holes, $|e| \cdot V_{s,max}$ where $V_{s,max}$ is the maximum of MEP in the hole, does not correlate with $E_{1/2}$ characterizing of EAA of the compounds (ESI). It might be considered as another indication that other effects are involved in the formation of RAs including spatial delocalization of their charge / spin.

Overall, the aforementioned arguments provide a reasonable explanation of the observed effect based on real-space delocalization. If so, the effect should be general, *i.e.*, embracing other heteroatom π-systems, with polyhalogenated benzenes being the natural referent system. Indeed, in the series C_6R_6 (R = F, Cl, Br, I) a gas-phase *v*EA_1 is positive and equal (experiment / CCCSD(T) + ZPE calculations) to 0.53 / 0.55, 0.92 / 0.86, – / 1.17, – / 1.82 eV, respectively (exp. for C_6H_6: –1.17 eV), *i.e.,* revealing the same χ_A-contradictive trend which, however, was not explained.[53] Accordingly, unexplained CV data reveal that amongst C_6F_6,[54] C_6Cl_6[55] and C_6Br_6[56] the former is the weakest, and the latter the strongest, one-electron acceptor (C_6I_6 was, seemingly, never studied due to very poor solubility in suitable solvents); for C_6R_6, $E_{1/2}$ = –2.49, –1.99 and –1.66 V (R = F, Cl and Br, respectively, *vs.* Fc / Fc$^+$ in DMF).[53-56]

Conclusion

Unexpectedly, the EAA of 2,1,3-benzochalcogenadiazoles **E/R** and **E/R'** (E = S, Se, Te; R = H, F, Cl, Br, I) increases with a decrease of electronegativity χ_A and electron affinity of E and R (except Cl) atoms; and for the halogenated derivatives, with a decrease of χ_M of molecules. DFT-calculated thermodynamics of the **E/R** + e$^{\cdot-}$ → [**E/R**]$^{\cdot-}$ electron capture in all cases reveal negative ΔG numerically increasing with the atomic numbers of both E and R atoms. The main driving force is ΔH, and positive ΔS has a minor influence. It is suggested that the discovered effect is caused by more effective charge / spin delocalization in heavier compounds due to contributions from diffuse (a real-space expanded) p-AOs of heavier E and R atoms. According to QTAIM and ELI-D, the transformation of **E/R** into [**E/R**]$^{\cdot-}$ also decreases the ionic character of the E–N bonds and increases the lone pair population of both E and N atoms.

The findings of this work clarify the previously unexplained situation with the EAA of C_6R_6 (R = F, Cl, Br, I) benzenes, amongst which C_6I_6 is a stronger electron acceptor than C_6F_6.[53-56]

It is expected that the discovered counterintuitive effect might be of the general character within main group chemistry and find applications in the design and synthesis of new functional materials. Particularly, **E/R** and **E/R'** heavier derivatives (E = Se, Te; R = Cl, Br, I) can be used in the design and synthesis of new CT complexes with tetrachalcogenafulvalenes (chalcogen = S, Se, Te) proposed as molecular (photo) conductors;[57,58] and, as in-chain or/and

pendant/side groups, in the design and synthesis of redox active ambipolar polymers for organic memristors.[4,5]

Overall, this work suggests that the scope of size-dependent effects in chemistry is broader than it is usually discussed,[59] and covers not only nanoparticles but also normal molecules with their isostructural / isoelectronic transformations. Notably, and in contrast to acenes,[43] the described increase of the EAA does not require an expansion of a molecular scaffold but only χ_A varying.

Experimental and Computational Section

General: The ^{13}C, ^{77}Se and ^{125}Te NMR spectra were measured with Bruker spectrometers AV-600, AV-400 and DRX-500 at frequencies of 150.9, 76.4 and 158.2 MHz, respectively; with standards TMS, Me_2Se and Me_2Te, respectively. High-resolution MS spectra were collected with a Thermo Scientific DFS instrument (EI, 70 eV); UV-Vis spectra, with Hewlett Packard Vectra VL and SF 2000 spectrophotometers; and IR spectra, with a Bruker Vector 22 spectrometer. Elemental analyses for C, N and S were accomplished with a CHNS-Analyzer Euro EA 300; and for Cl and Br, with mercurimetric titration of halides in the combustion products using diphenylcarbazone as an indicator. Simultaneous TG / DSC measurements were performed with a NETZSCH STA 409 instrument and *NETZSCH Proteus Thermal Analysis* software. GC-MS measurements were carried out with a Hewlett-Packard G1800A instrument combining HP 5890 Series II gas chromatograph (equipped with capillary column HP-5) and HP 5971 mass-selective detector (EI, 70 eV), or with an Agilent 6890N chromatograph combined with an Agilent 5973N system; with helium, 1 ml min^{-1}, as carrier gas.

Compounds **S/H**, **Se/H**, N-bromosuccinimide (NBS) and N-iodosuccinimide (NIS) were received from Aldrich and additionally purified by sublimation *in vacuo* or recrystallization. Compounds **Te/H**,[60,61] **S/F**,[62,63] **Se/F**,[62,63] **Te/F**,[64,65] **S/Cl**[66] and **Se/Cl**[66] were prepared and purified by known methods.

Syntheses: Compound S/Br: At ambient temperature, 4.83 g (27 mmol) of NBS were added slowly in portions to a stirred solution of 0.616 g (4.5 mmol) of **S/H** in 20 ml of concentrated sulfuric acid in 50-ml flask. The flask was closed with a stopper, and the reaction mixture was stirred for 96 h and poured into 50 ml of water. The yellow precipitate was filtered off, washed with concentrated aqueous Na_2SO_3 and then H_2O till neutral reaction of washing water. The product was dried *in vacuo* overnight. Compound **S/Br** was obtained in the form of off-white powder, 1.24 g (61%), m. p. 230-231 °C (225-227 °C).[67] Found / calculated for $C_6Br_4N_2S$, %: C 15.97 / 15.95, Br 70.97 / 70.75, N 6.18 / 6.20, S 7.07 / 7.10 (GC-MS purity > 99%). MS, measured / calculated for $C_6{}^{79}Br_3{}^{81}Br{}^{14}N_2{}^{32}S$: 449.6492 / 449.6489. ^{13}C NMR (d_6-Me_2S=O), δ, ppm: 151.5, 129.7, 117.2. UV-Vis ($CHCl_3$), λ_{max}, nm, (log ε): 247 (4.15), 323 (4.10), 337 (4.17), ~360 (3.67, shoulder) (ESI). Single crystals suitable for XRD were obtained by slow diffusion of pentane vapor into toluene solution of **S/Br** at ambient temperature.

Compound Se/Br: At ambient temperature, 4.33 g (24 mmol) of NBS were added slowly in portions to a stirred solution of 0.430 g (2.4 mmol) of **Se/H** in 10 ml of concentrated sulfuric acid in a 25-ml flask. The flask was closed with a stopper, and reaction mixture was stirred at for 72 h and poured into 100 ml of ice. The yellow precipitate was filtered off, washed with H_2O until neutral reaction of washing water. The product was dried *in vacuo* overnight. Compound **Se/Br** was obtained in the form of yellow powder, 0.312 g (27%); on heating, **Se/Br** decomposes without melting after ~300 °C (TG / DSC; ESI). Found / calculated for $C_6Br_4N_2Se$, %: C 14.46 / 14.45, Br 63.33 / 64.09, N 5.61 / 5.62 (GC-MS purity > 99%). MS, measured / calculated for $C_6{}^{79}Br_4N_2{}^{80}Se$: 495.5958 / 495.5955. NMR (d_6-Me_2S=O), δ, ppm: ^{13}C: 171.1, 156.7, 143.8; ^{77}Se: 1542 (ESI). UV-Vis ($CHCl_3$), λ_{max}, nm, (log ε): 245 (4.07), 303 (4.25), 344 (3.91), 358 (4.00), ~387 (3.31, shoulder) (ESI). Single crystals suitable for XRD were obtained by slow evaporation of solution of **Se/Br** in toluene.

Compound Te/Cl: At ambient temperature and under argon, a solution of 0.681 g (2.5 mmol) of $TeCl_4$ in 20 ml of toluene was added dropwise to a stirred solution of 1,2-diamino-3,4,5,6-tetrachlorobenzene[66] in 100 ml of the same solvent. After 1 h, 2 ml (14.4 mmol) of Et_3N were added to the orange reaction mixture. After additional 0.5 h, the precipitate was filtered off, and the solution was concentrated at the reduced pressure. The solid residue was washed with CH_2Cl_2 to remove traces of $Et_3NH^+Cl^-$, recrystallized from hot Me_2S=O and dried for 3 h at 50°C *in vacuo*. Compound **Te/Cl** was obtained in the form of yellow thin needles, 0.706 g (76%); on heating, **Te/Cl** decomposes without melting after ~300 °C (TG / DSC; ESI). Found / calculated for $C_6Cl_4N_2Te$, %: C 19.30 / 19.50, Cl 37.75 / 38.38, N 7.12 / 7.53. MS, measured / calculated for $C_6{}^{35}Cl_3{}^{37}Cl{}^{126}N_2Te$: 369.7818 / 369.7821. NMR (d_6-Me_2S=O), δ, ppm: ^{13}C: 132.2, 116.9, 113.6; ^{125}Te: 2431 (ESI). UV-Vis (THF), λ_{max}, nm, (log ε): 218 (4.40), 405 (4.34) (ESI). IR (KBr), ν, cm^{-1}: 1616 m, 1548 w, 1463 s, 1398 m, 1349 w, 1319 m, 1261 s, 1203 vs, 1139 w, 1014 w, 975 m, 811 c, 700 c, 626 m, 584 s, 466 m, 437 w. Solvate **Te/Cl** · Me_2S=O in the form of prismatic single crystals suitable for XRD was obtained by storing of **Te/Cl** under Me_2S=O for several weeks at ambient temperature.

Compound S/Br': At ambient temperature, a stirred solution of 1.02 g (7.5 mmol) of **S/H** and 2.80 g (15.8 mmol) of NBS in 25 ml of concentrated H_2SO_4 was kept for 24 h in a firmly closed flask. The reaction mixture was poured into 100 ml of ice, and the precipitate was filtered off, washed twice with water, dried *in vacuo* overnight, and recrystallized from 130 ml of 4 : 1 hexane / toluene. Compound **S/Br'**[68,69] was obtained in the form of colorless needles, 1.61 g (73%). ^1H NMR ($CDCl_3$), δ, ppm: 7.72.

Compound Se/Br': At ambient temperature, a stirred solution of 10.00 g (54.6 mmol) of **Se/H** and 19.60 g (110.1 mmol) of NBS in 230 ml of concentrated H_2SO_4 was kept for 24 h in a firmly closed flask. The reaction mixture was poured into 1 liter of ice and the precipitate was filtered off, washed carefully with water and dried *in vacuo* over two days. Compound **Se/Br'**[69] was obtained in the form of green-yellow powder, 17.05 g (92%; GC-MS purity > 95%). ^1H NMR ($CDCl_3$), δ, ppm: 7.64. Sample for CV measurements was prepared by crystallization from toluene (GC-MS purity > 98%).

Compound Te/Br': At ambient temperature and under argon, a solution of 0.253 g (0.9 mmol) of $TeCl_4$ in 20 ml of pyridine was added dropwise to a stirred solution of 0.250 g (0.9 mmol) of 3,6-dibromo-1,2-benzenediamine in 20 ml of the same solvent. After 0.5 h, 1 ml (7.2 mmol) of Et_3N was added to the orange reaction mixture; and after additional 0.5 h, the solvent was removed at the reduced pressure. The solid residue was mixed with 50 ml of MeCN to remove $Et_3NH^+Cl^-$, the mixture was filtered, and the filter cake washed twice with additional 10 ml of MeCN and dried *in vacuo*. Compound **Te/Br'**[61] was obtained in the form of orange powder, 0.336 g (87%). NMR ($CDCl_3$), δ, ppm: ^1H: 7.56. Found / calculated for $C_6Br_2N_2Te$, %: C 18.92 / 18.50, H 0.50 / 0.52, N 6.97 / 7.19.

Compound S/I': At ambient temperature and under argon, 14.22 g (56.0 mmol) of I_2 in one portion, and then 23.81 g (76.3 mmol) of Ag_2SO_4 in small portions, were added to a stirred solution of 3.46 g (25.4 mmol) of **S/H** in 80 ml of concentrated H_2SO_4 (this order of addition provides homogeneous solution and prevents clumping of the solid reagents). The reaction mixture was kept at 100 °C for 48 h, cooled to the room temperature and poured into 600 ml of ice. The precipitate was washed carefully with water and dried *in vacuo* overnight. The obtained solid was extracted 3×300 ml of boiling DCM, and combined extract was evaporated to dryness. Compound **S/I'**[70,71] was obtained in the form of yellow needles, 8.26 g (84%). NMR (d_6-Me_2S=O), δ, ppm: ^1H: 7.79; ^{13}C: 152.8, 132.2, 113.7.

Compound Se/I': Under argon, a stirred mixture of 0.50 g (1.5 mmol) of **Se**/**Br'**, 2.50 g (13.2 mmol) of CuI and 4.32 g (26.0 mmol) of KI with 20 ml of DMF was kept at 150 °C for 48 h. The reaction mixture was cooled to the ambient temperature, poured into 70 ml of water and the brown precipitate was filtered off. This product was suspended in 100 ml of 20% aqueous ammonia, stirred at ambient temperature for 30 min and filtered off. The yellow solid was washed with water, dried *in vacuo* overnight, sublimed at 170 °C / 4×10^{-2} Torr, and recrystallized from ethylacetate. Compound **Se/I'**[72] (GC-MS: 95%) was obtained in the form of bright-yellow needles, 0.12 g (19%). NMR (d_6-Me_2S=O), δ, ppm: ^{1}H: 7.81; ^{13}C: 157.0, 139.4, 92.9.

Compound Te/I': *a*) At 0° C and under argon, 0.59 g (15.5 mmol) of $NaBH_4$ and 0.024 g (0.1 mmol) of $CoCl_2\cdot6H_2O$ were added consequently to a stirred solution of 2.00 g (5.2 mmol) of **S/I'** in a mixture of 30 ml of ethanol and 10 ml of THF. The reaction mixture was kept at ambient temperature for 5 h (longer reaction times led to deiodination), and the black precipitate was filtered off and carefully washed with ethanol. The filtrate was evaporated to dryness, and the residue was mixed with 10 ml of water, stirred for 20 min, filtered off, and dried *in vacuo*. 3,6-Diiodo-1,2-benzenediamine[72] was obtained in the form of yellow solid, 0.80 g (43%). NMR ($CDCl_3$), δ, ppm: ^{1}H: 6.69 (2H), 4.88 (4H). *b*) At ambient temperature and under argon, a solution of 0.214 g (0.8 mmol) of $TeCl_4$ in 10 ml of pyridine was added dropwise to a stirred solution of 0.287 g (0.8 mmol) of the diamine in 10 ml of the same solvent. After 0.5 h, 1 ml (7.2 mmol) of Et_3N was added to the orange reaction mixture. After additional 0.5 h, the solvent was removed at the reduced pressure. The solid residue was mixed with 30 ml of MeCN, the mixture was filtered, the filter cake washed twice with additional 5 ml of MeCN and dried *in vacuo*. Compound **Te/I'**[73] was obtained in the form of red powder, 0.336 g (87%). NMR (d_6-Me_2S=O), δ, ppm: ^{1}H: 7.61 (2H); ^{13}C: 161.3, 137.7, 102.5; ^{125}Te: 2340 (ESI); ^{1}H and ^{13}C NMR spectra correspond to published.[73] Found / calculated for $C_6I_2N_2Te$, %: C 15.22 / 14.90, H 0.57 / 0.42, N 5.62 / 5.79.

X-ray crystallography: The crystallographic data for compounds **S**/**Br**, **Se**/**Br** and **Te**/**Cl**·Me_2S=O (Figure 3; ESI) were collected with a Bruker Kappa Apex II CCD diffractometer by using a graphite-monochromated MoKα irradiation. The structures were solved by direct method using the *SHELX-97* program[74,75] and refined by full-matrix least-squares method against all F^2 in anisotropic approximation using the *Olex2* program.[76] The H atoms positions were calculated with the riding model. Absorption corrections were applied using the empirical multiscan method with the *SADABS* programs.[77] The obtained crystal structures were analysed for shortened contacts between non-bonded atoms using the *PLATON*[78,79] and *MERCURY*[80] programs. Atomic coordinates, thermal parameters, bond lengths, and bond angles were deposited at the Cambridge Crystallographic Data Center. CCDC 2165320 (**S**/**Br**), 2165319 (**Se**/**Br**), and 2165318 (**Te**/**Cl**·Me_2S=O) contain the supplementary crystallographic data for this paper. These data can be obtained free of charge from The Cambridge Crystallographic Data Centre.

Cyclic voltammetry and electron paramagnetic resonance: CV measurements (ESI) were performed at 293 K with a PG 310 USB potentiostat (HEKA Elektronik GmbH, Germany) for DMF and MeCN solutions using a standard glass electrochemical cell (solution volume of 5 mL) equipped with a stationary Pt disc working electrode (A = 0.0143 cm^2, calibrated using ferrocene as a standard). Pt helix was used as an auxiliary electrode. The solutions were bubbled with dry argon to remove air. The cell was connected to the potentiostat using a three-electrode circuit. Peak potentials were quoted with a reference to a saturated calomel electrode (SCE). A bridge with 0.1 M of MeCN solution of n-Bu_4NClO_4 supporting electrolyte was used to connect the cell and SCE. Combined electrochemical / EPR measurements (ESI) were accomplished with an ELEXSYS E-540 spectrometer (X-band, MW frequency ca. 9.87 GHz, MW power 1 mW, modulation frequency 100 kHz, and modulation amplitude 0.006 mT) equipped with a high-Q cylindrical resonator ER4119HS. An electrochemical cell for EPR measurements equipped with Pt working electrode, Pt auxiliary electrode and pseudo-reference Ag/AgCl electrode for organic solvents was used. The working electrode was placed into the EPR cavity. Electrolysis was performed using potentiostatic mode in anhydrous DMF and MeCN with 0.1 M Et_4NClO_4 as a supporting electrolyte. Simulations of the experimental EPR spectra were accomplished with the *Winsim 2002* program.[81] The *Simplex* algorithm was used for optimization of hfc constants and line widths.

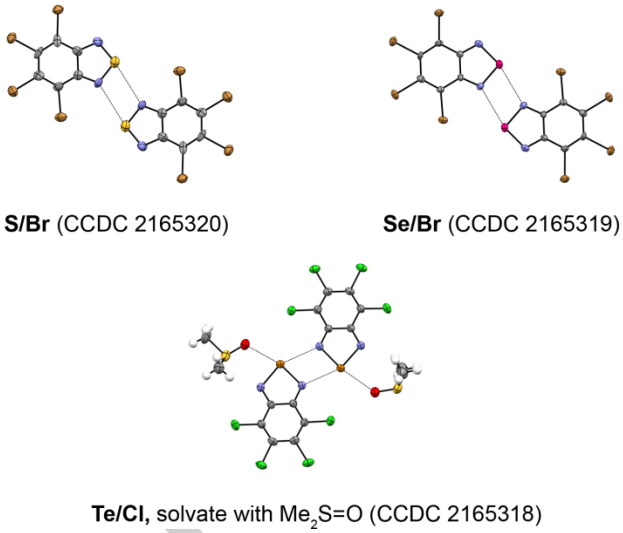

Figure 3. XRD molecular structures of compounds **S**/**Br**, **Se**/**Br** and **Te**/**Cl**·Me_2S=O (displacement ellipsoids at 30%); color code: C – grey, H – light grey, Cl – green, Br – brown, N – blue, O – red, S – yellow, Se – magenta, Te – orange.

Quantum chemical calculations: DFT calculations were performed with the *GAUSSIAN16*[82] and *Orca 5.0.2*[83] suits of programs applying (U)B3LYP and (U)B97-D3 functionals and def2-tzvp basis set with ECP for Te and I.[84-90] Thermodynamics of the **E**/**R** + $e^{\cdot-}$ → [**E**/**R**]$^{\cdot-}$ electron capture was calculated at the (U)B97-D3/def2-tzvp level of theory with the Becke-Johnson damping scheme (D3BJ)[91] and gCP correction,[92] and refers to T = 298.15 K and P = 1 atm. The DFT wavefunctions were employed in the QTAIM analysis with the *AIMAll* program,[93] whereas the *DGrid* program[94] was used to generate and analyze the ELI-D real-space bonding descriptors applying a grid step size of 0.05 a. u. The ELI-D and QTAIM results were visualized with the *Multiwfn_3.8*[95] and *VMD*[96] programs.

Acknowledgements

The authors are grateful to Yana A. Ponomareva for participation in syntheses and Dr. Inna K. Shundrina for TG / DSC measurements; as well as to the Deutsche Forschungsgemeinschaft (project BE 3716/6-2, formulation of the problem and ELI-D calculations), Russian Foundation for Basic Research (project 20-33-90-232, syntheses and XRD measurements), Commission for Grants of the President of the Russian Federation (project MK-1533.2021.1.3, DFT and QTAIM calculations) and Russian Science Foundation (project 22-13-00108, electrochemical and EPR measurements; project 21-73-10291, MEP calculations) for financial support. They are also grateful to the Multi-Access Chemical Research Center and Siberian Supercomputer Center, Siberian Branch of the Russian Academy of Sciences, for instrumental and computational facilities, respectively.

Conflicts of Interest

There are no conflicts to declare.

Data Availability Statement

The data that support the findings of this study are available in the electronic supplementary information (ESI) of this article including XRD, NMR, UV-Vis, TG / DSC, CV, EPR, DFT, QTAIM, ELI-D and MEP data. See DOI: 10.1002/chem.xxxxxxxxx

Keywords: chalcogen-nitrogen compounds • halogen compounds • heteroatom π-systems • main group chemistry • molecular electron affinity

[1] H. J Wörner, C. A. Arrell, N. Banerji, A. Cannizzo, M. Cherqui, A. K. Das, P. Hamm, U. Keller, P. M. Kraus, E. Liberatore, P. Lopez-Tarifa, M. Luccini, M. Meuwly, C. Milne, J.-E. Moser, U. Rothlisberger, G. Smolentsev, J. Teuscher, J. A. van Bockhoven, O. Wenger, *Struct. Dyn.* **2017**, *4*, 061508.

[2] Y. Mao, Q. Ge, P. R. Horn, M. Head-Gordon, *J. Chem. Theory Comput.* **2018**, ***14***, 2401–2417.

[3] K. P. Goetz, D. Vermeulen, M. E. Payne, C. Kloc, L. E. McNeil, O. D. Jurchescu, *J. Mater. Chem. C* **2012**, *2*, 3065–3076.

[4] W.-P. Lin, S.-J. Liu, T. Gong, Q. Zhao and W. Huang, *Adv. Mater*. **2014**, *26*, 570–606.

[5] D. S. Odintsov, I. K. Shundrina, I. A. Os'kina, I. V. Oleynik, J. Beckmann, L. A. Shundrin, *Polym. Chem.* **2020**, *11*, 2243–2251.

[6] V. Coropceanu, XK. Chen, T. Wang, Z. Zheng, J.-L. Bredas, *Nat. Rev. Mater.* **2019***, 4*, 689–707.

[7] C. Tantardini, A. R. Oganov, *Nat. Commun.* **2021**, *12*, 2087 (the article contains misleading claim on dimensionality of actually dimensionless Pauling electronegativity).

[8] M. Marco-Perez, J. L. Garquez, *J. Phys. Chem. A* **2019**, *123*, 10065–10071.

[9] M. V. Putz, *Cur. Phys. Chem.* **2011**, *1*, 111–139.

[10] R. S. Mulliken, *J. Chem. Phys.* **1934**, *2*, 782–793.

[11] J. B. Mann, T. L. Meek, L. C. Allen, *J. Am. Chem. Soc.* **2000**, *122*, 2780–2783.

[12] E. A. Pritchina, N. P. Gritsan, O. A. Rakitin, A. V. Zibarev, *Targets Heterocycl. Syst.* **2019**, *23*, 143–154.

[13] T. Chivers, R. S. Laitinen, *Chalcogen-Nitrogen Chemistry: From Fundamentals to Applications in Biological, Physical, and Materials Sciences*, World Scientific, 2021.

[14] O. A. Rakitin, in: *Comprehensive Heterocyclic Chemistry IV*, Elsevier, 2022, Vol. 5, pp. 372–406.

[15] S. Yamazaki, in: *Comprehensive Heterocyclic Chemistry IV*, Elsevier, 2022, Vol. 6, pp. 303–409.

[16] S. Kolb, G. A. Oliver, B. Werz, in *Comprehensive Inorganic Chemistry III*, Elsevier, 2023. https://doi.org/10.1016/B978-0-12-823144-9.00059-5

[17] B. A. D. Neto, J. R. Correa, J. Spencer, *Chem. Eur. J.* **2022**, *28*, e202103262.

[18] O. A. Rakitin, A. V. Zibarev, *Asian J. Org. Chem.* **2018**, *7*, 2397–2416.

[19] E. A. Chulanova, N. A. Semenov, N. A. Pushkarevsky, N. P. Gritsan, A. V. Zibarev, *Mendeleev Commun.* **2018**, *28*, 453–460.

[20] L. A. Robertson, I. A. Shkrob, G. Agarwal, Y. Zhao, Z. Yu, R. S. Assary, L. Cheng, J. S. Moore, L. Zhang, *ACS Energy Lett.* **2020**, *5*, 3062–3068.

[21] N. A. Pushkarevsky, A. I. Smolentsev, A. A. Dmitriev, I. Vargas-Baca, N. P. Gritsan, J. Beckmann, A. V. Zibarev, *Chem. Commun.* **2020**, *56*, 1113–1116.

[22] E. A. Chulanova, E. A. Radiush, I. K. Shundrina, I. Yu. Bagryanskaya, N. A. Semenov, J. Beckmann, N. P. Gritsan, A. V. Zibarev, *Cryst. Growth Des.* **2020**, *20*, 5868–5879.

[23] N. A. Pushkarevsky, E. A. Chulanova, L. A. Shundrin, A. I. Smolentsev, G. E. Salnikov, E. A. Pritchina, A. M. Genaev, I. G. Irtegova, I. Yu. Bagryanskaya, S. N. Konchenko, N. P. Gritsan, J. Beckmann, A. V. Zibarev, *Chem. Eur. J.* **2019**, *25*, 806–816.

[24] A. V. Zibarev, in: *Chalcogen Chemistry: Fundamentals and Applications*, Royal Society of Chemistry, 2023, in press.

[25] E. A. Chulanova, E. A. Pritchina, L. A. Malaspina, S. Grabowsky, F. Mostaghimi, J. Beckmann, I. Yu. Bagryanskaya, M. V. Shakhova, L. S. Konstantinova, O. A. Rakitin, N. P. Gritsan, A. V. Zibarev, *Chem. Eur. J.* **2017**, *23*, 852–864.

[26] A. V. Zibarev, R. Mews, in: *Selenium and Tellurium Chemistry: From Small Molecules to Biomolecules and Materials*, Springer, 2011.

[27] E. R. T. Tiekink, *Coord. Chem. Rev.* **2022**, *457*, 214397.

[28] P. C. Ho, J. Z. Wang, F. Meloni, I. Vargas-Baca, *Coord. Chem. Rev.* **2020**, *422*, 213464.

[29] R. T. Boere, T. L. Roemmele, *Coord. Chem. Rev.* **2000**, *210*, 369–445.

[30] Onset potential E_{on} is the potential at which a specific process begins as revealed by an increase in current in a current-potential *i-E* curve. As a measure of the EAA in the series of related compounds, E_{on} can be used when measured under the same electrochemical conditions covering working electrode material, potential sweep rate and temperature.

[31] W. Alhalasah, R. Holze, *J. Solid State Electrochem.* **2007**, 11, 1605–1612.

[32] J. Heinze, B. A. Frontana-Uribe, S. Ludwigs, *Chem Rev.* **2010**, *110*, 4724–4771.

[33] A. F. Cozzolino, N. E. Gruhn, D. L. Lichtenberger, I. Vargas-Baca, *Inorg. Chem.* **2008**, *47*, 6220–6226.

[34] N. E. Petrachenko, V. I. Vovna, A. V. Zibarev, G. G. Furin, *Chem. Heterocycl. Compd.* **1991**, **27**, 451–454.

[35] A. Streitwieser, *Molecular Orbital Theory for Organic Chemists*, Wiley, 1961.

[36] J. C. Rienstra-Kiracofe, G. S. Tschumper, H. F. Schaefer, S. Nandi, G. B. Ellison, *Chem. Rev.* **2002**, *102*, 231–282.

[37] P. Kebarle, S. Chowdhury, *Chem. Rev*. **1987**, *87*, 513–534.

[38] B. Cordero, V. Gomez, A. E. Platero-Prats, M. Reves, J. Echeverria, E. Cremades, F. Barragan, S. Alvarez, *Dalton Trans.* **2008**, 2832–2838.

[39] S. Alvarez, *Dalton Trans.* **2013**, *42*, 8617–8636.

[40] [M. Mantina, A. C. Chamberlin, R. Valero, C. J. Cramer, D. G. Truhlar, *J. Phys. Chem. A* **2009**, *113*, 5806–5812.

[41] I. Yu. Chernyshov, I. V. Ananyev, E. A. Pidko, *ChemPhysChem* **2020**, *21*, 370–376

[42] S. Fujisawa, K. Ohno, S. Masuda, Y. Harada, *J. Am. Chem. Soc.* **1986**, *108*, 6505–6511.

[43] L. D. Betowski, M. Enlow, L. Riddick, D. H. Aue, *J. Phys. Chem. A* **2006**, *110*, 12927–12946.

[44] A. Szabo, N. O. Ostlund*, Modern Quantum Chemistry: Introduction to Advanced Electronic Structure Theory,* Dover, 1996.

[45] R. W. F. Bader, *Atoms in Molecules*: *A Quantum Theory*, Cambridge University Press, 1991.

[46] S. Shahbazian, *Int. J. Quant. Chem.* **2018**, *118*, e25637.

[47] The E atoms are much more positive, and the N atoms more negative, in the QTAIM framework; the atoms C3*a* and C7*a* (Scheme 1) are practically neutral on the Mulliken scale but have positive charges q = ~0.5 on the QTAIM scale. The QTAIM shows that the **E/R** + e^{-} → [**E/R**]$^{-}$ electron capture mainly affects q's of the E and R atoms in the order S > Se ~ Te, and R = H ~ F > Cl > Br (ESI). Thus, the S atom has q = 1.24 in **S/F** and q = 0.75 in [**S/F**]$^{-}$; and a difference Δq = –0.53 suggests that approximately half of the added electron is localized at the S atom. With the Se and Te atoms, Δq = –0.36 (**Se/F** *vs.* [**Se/F**]$^{-}$) and –0.37 (**Te/F** *vs.* [**Te/F**]$^{-}$). For R = I, Δq = –0.18 (**S/I** *vs.* [**S/I**]$^{-}$), –0.19 (**Se/I** *vs.* [**Se/I**]$^{-}$) and –0.23 (**Te/I** *vs.* [**Te/I**]$^{-}$).

[48] M. Kohout, *Int. J. Quantum Chem.* **2004**, *97*, 651–658.

[49] M. Kohout, F. R. Wagner, Y. Grin, *Theor. Chem. Acc.* **2008**, 119, 413–420.

[50] S. Shahbazian, *Chem. Eur. J.* **2018**, *24*, 5401–5405.

[51] *Chemical Applications of Atomic and Molecular Electrostatic Potentials,* eds. P. Politzer and D. G. Truhlar, Springer, 1981.

[52] P. Politzer, J. S. Murray, *J. Comput. Chem.* **2018**, *39*, 464-471.

[53] F. Volaton, C. Roche, *Chem. Phys. Lett.* **2007**, *446*, 243–249.

[54] CV data for C_6F_6 were not found in literature; in this work, its $E_{1/2}$ in DMF was evaluated via the E_{on} potential of one-electron reduction (ESI).
[55] P. P. Romanczyk, G. Rotko, S. S. Kurek, *Phys. Chem. Chem. Phys.* **2016**, *18*, 22573.
[56] G. Rotko, P. P. Romanczyk, G. Andryianau, S. S. Kurek, *Electrochem. Commun.*, **2014**, *43*, 117–120.
[57] N. A. Pushkarevsky, A. V. Lonchakov, N. A. Semenov, E. Lork, L. I. Buravov, L. S. Konstantinova, G. T. Silber, N. Robertson, N. P. Gritsan, O. A. Rakitin, J. D. Woollins, E. B. Yagubskii, J. Beckmann, A. V. Zibarev, *Synth. Met.* **2012**, *162*, 2267–2276.
[58] E. A. Chulanova, E. A. Radiush, Y. Balmohammadi, S. Grabowsky, J. Beckmann, A. V. Zibarev, *CrystEngComm* **2023**, *25*. https://doi.org/10.1039/d2ce01385a
[59] E. Roduner, *Chem. Soc. Rev.* **2006**, *35*, 583–592.
[60] N. A. Pushkarevsky, P. A. Petrov, D. S. Grigoriev, A. I. Smolentsev, L. M. Lee, F. Kleemiss, G. E. Salnikov, S. N. Konchenko, I. Vargas-Baca, S. Grabowsky, J. Beckmann, A. V. Zibarev, *Chem. Eur. J.* **2017**, *23*, 10987–10991.
[61] A. F. Cozzolino, J. F. Britten, I. Vargas-Baca, *Cryst. Growth Des.* **2006**, *6*, 181–186.
[62] A. G. Makarov, N. Yu. Selikhova, A. Yu. Makarov, V. S. Malkov, I. Yu. Bagryanskaya, Yu. V. Gatilov, A. S. Knyazev, Yu. G. Slizhov, A. V. Zibarev, *J. Fluor. Chem.* **2014**, *165*, 123–131.
[63] A. V. Zibarev, A. O. Miller, *J. Fluor. Chem.* **1990**, *50*, 359–363.
[64] A. F. Cozzolino, P. S. Whitfield, I. Vargas-Baca, *J. Am. Chem. Soc.* **2010**, *132*, 17265–17270.
[65] V. N. Kovtonyuk, A. Yu. Makarov, M. M. Shakirov, A. V. Zibarev, *Chem. Commun*. **1996**, 1991–1992.
[66] D. O. Prima, E. V. Vorontsova, A. G. Makarov, A. Yu. Makarov, I. Yu. Bagryanskaya, T. F. Mikhailovskaya, Yu. G. Slizhov, A. V. Zibarev, *Mendeleev Commun.* **2017**, *27*, 439–442.
[67] C. Ceriani, F. Corsini, G. Mattoli, S. Mattiello, D. Testa, R. Po, C. Batta, G. Graffini, L. Berita, *J. Mater. Chem. C* **2021**, *9*, 14815–14826.
[68] K. Pilgram, M. Zupan, R. Skiles, *J. Heterocycl. Chem.* **1970**, **7**, 629–633.
[69] E. A. Knyazeva, O. A. Rakitin, *Chem. Heterocycl. Comp.* **2017**, *53*, 855–857.
[70] M. Shimada, M. Tsuchiya, R. Sakamoto, Y. Yamanoi, E. Nishibori, K. Sugimoto, H. Nishihara, *Angew. Chem. Int. Ed.* **2016**, *55*, 3022–3026.
[71] D. M. Gampe, S. Schramm, F. Nöller, D. Weiß, H. Görls, P. Naumov, R. Beckert, *Chem. Commun.* **2017**, *53*, 10220–10223.
[72] Y. Tsubata, T. Suzuki, T. Miyashi, Y. Yamashita, *J. Org. Chem.* **1992**, *57*, 6749–6755.
[73] Ishigaki, K. Shimomura, K. Asai, T. Shimajiri, T. Akutagawa, T. Fukushima, T. Suzuki, *Bull. Chem. Soc. Jpn* **2022**, *95*, 522–531.
[74] G. M. Sheldrick, *SHELX-97 – Programs for Crystal Structure Analysis (Release 97-2)*, University of Göttingen, Germany, 1997.
[75] G. M. Sheldrick, *Acta Crystallogr. C* **2015**, *71*, 3–8.
[76] O. V. Dolomanov, L. J. Bourhis, R. J. Gildea, J. A. K. Howard, H. Puschmann, *J. Appl. Crystallogr.* **2009**, *42*, 339–341.
[77] *SADABS, v. 2008-1*, Bruker AXS Inc., Madison, WI, USA, 2008.
[78] A. L. Spek, *PLATON, A Multipurpose Crystallographic Tool (Version 10M)*, Utrecht University, Utrecht, The Netherlands, 2003.
[79] A. L. Spek, *J. Appl. Crystallogr.* **2003**, *36*, 7–13.
[80] C. F. Macrae, P. R. Edgington, P. McCabe, E. Pidcock, G. P. Shields, R. Taylor, M. Towler, J. van de Streek, *J. Appl. Crystallogr.* **2006**, *39*, 453–457.
[81] D. R. Duling, *J. Magn. Reson. B* **1994**, *104*, 105–110.
[82] *Gaussian 16, Revision C.01*, M. J. Frisch, G. W. Trucks, H. B. Schlegel, G. E. Scuseria, M. A. Robb, J. R. Cheeseman, G. Scalmani, V. Barone, G. A. Petersson, H. Nakatsuji, X. Li, M. Caricato, A. V. Marenich, J. Bloino, B. G. Janesko, R. Gomperts, B. Mennucci, H. P. Hratchian, J. V. Ortiz, A. F. Izmaylov, J. L. Sonnenberg, D. Williams-Young, F. Ding, F. Lipparini, F. Egidi, J. Goings, B. Peng, A. Petrone, T. Henderson, D. Ranasinghe, V. G. Zakrzewski, J. Gao, N. Rega, G. Zheng, W. Liang, M. Hada, M. Ehara, K. Toyota, R. Fukuda, J. Hasegawa, M. Ishida, T. Nakajima, Y. Honda, O. Kitao, H. Nakai, T. Vreven, K. Throssell, J. A. Montgomery, Jr., J. E. Peralta, F. Ogliaro, M. J. Bearpark, J. J. Heyd, E. N. Brothers, K. N. Kudin, V. N. Staroverov, T. A. Keith, R. Kobayashi, J. Normand, K. Raghavachari, A. P. Rendell, J. C. Burant, S. S. Iyengar, J. Tomasi, M. Cossi, J. M. Millam, M. Klene, C. Adamo, R. Cammi, J. W. Ochterski, R. L. Martin, K. Morokuma, O. Farkas, J. B. Foresman, D. J. Fox, Gaussian Inc., Wallingford CT, 2019.
[83] F. Neese, F. Wennmohs, U. Becker, C. Riplinger, *J. Chem. Phys.* **2020**, *152*, 224108.
[84] F. Weigend, *Phys. Chem. Chem. Phys.* **2006**, *8*, 1057–1065.
[85] A. D. Becke, *J. Chem. Phys.* **1993**, *98*, 5648–5652.
[86] C. Lee, W. Yang, R. G. Parr, *Phys. Rev. B* **1988**, *37*, 785–789.
[87] F. Weigend, R. Ahlrichs, *Phys. Chem. Chem. Phys.* **2005**, *7*, 3297–3305.
[88] A. Schaefer, H. Horn, R. Ahlrichs, *J. Chem. Phys*. **1992**, *97*, 2571–2577.
[89] S. Grimme, S. Ehrlich, L. Goerigk, *J. Comput. Chem.* **2011**, *32*, 1456–1465.
[90] N. Mardirossian, M. Head-Gordon, *Mol. Phys.* **2017**, *115*, 2315–2372.
[91] S. Grimme, J. Antony, S. Ehrlich, H. Krieg, *J. Chem. Phys.* **2010**, *132*, 154104.
[92] H. Kruse, S. Grimme, *J. Chem. Phys.* **2012**, *136*, 154101.
[93] T. A. Keith, *AIMAll, Version 15.09.27*, TK Gristmill Software, Overland Park KS, USA, 2015 (aim.tkgristmill.com).
[94] M. Kohout, *DGrid, Version 5.1*, Dresden, Germany, 2019.
[95] T. Lu, F. Chen, *J. Comput. Chem.* **2012**, *33*, 580–592.
[96] W. Humphrey, A. Dalke, K. Schulten, *J. Mol. Graph.* **1996**, *14*, 33–38.

Entry for the Table of Contents

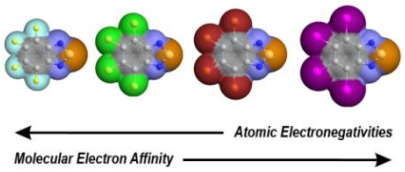

The size does matter: Changing in 2,1,3-benzochalcogenadiazoles $C_6R_4N_2E$ and $C_6H_2R_2N_2E$ (E = S, Se, Te; R = H, F, Cl, Br, I) lighter / smaller E and non-hydrogen R atoms to heavier / bigger, *i.e.*, decreasing atomic electronegativities, increases molecular electron affinities.